# Fabrication of $ZnSnP_2$ thin films by phosphidation

**S. Nakatsuka, Y. Nose*, T. Uda**

Department of Materials Science and Engineering, Kyoto University, Yoshida-Honmachi, Sakyo-ku, Kyoto, 606-8501, Japan

*Corresponding author

nose.yoshitaro.5e@kyoto-u.ac.jp

## Abstract

$ZnSnP_2$ is a promising candidate as a solar absorber material consisting of earth-abundant and low-toxic elements. In this study, the phosphidation method, where co-sputtered Zn-Sn thin films react with phosphorus gas, was adopted as a new method for fabricating $ZnSnP_2$ thin films. The influence of phosphidation temperature on product phases was investigated, and the reaction route to obtain $ZnSnP_2$ was discussed using chemical potential diagrams of the Zn-Sn-P system. It was clarified that Zn preferentially reacted with phosphorus gas at the initial stage of phosphidation. $ZnSnP_2$ thin films with a single phase were successfully obtained by phosphidation at 500 °C for 30 min under a phosphorus partial pressure of $10^{-2}$ atm. However, the formation of $ZnSnP_2$ protrusions was observed on the surface of the thin films. It was concluded that liquid Sn particles extruded to the surface reacted with $Zn_3P_2$ and phosphorus gas to form $ZnSnP_2$ protrusions, and the way to improve the surface

morphology was proposed.

## 1. Introduction

In recent years, various types of solar cells have been investigated due to increasing energy demand and low cost. Among them, $CuIn_{1-x}Ga_xSe_2$ (CIGS) and CdTe show high conversion efficiencies of 20.8% and 20.4%, respectively. [1] However, it is undesirable to use toxic elements, Cd and Te, or rare elements, In and Ga. With these considerations in mind, solar absorbing materials consisting of earth-abundant and low-toxicity elements have been pursued. Solar cells using $Cu_2ZnSnS_{4-x}Se_x$ (CZTS), which was fabricated by a solution process based on hydrazine, achieved the conversion efficiency of 12.6% [2], however it is not sufficient compared to CIGS solar cells. Therefore, $ZnSnP_2$ with a chalcopyrite structure was investigated as an alternative candidate for a solar absorber in this paper. $ZnSnP_2$ consists of safe and abundant elements and its direct bandgap is 1.66 eV [3], which is suitable from the viewpoint of the theoretical conversion efficiency based on the Shockley-Queisser limit [4]. In addition, a high absorption coefficient of around $10^5$ $cm^{-1}$ was reported for visible light. [5] Thus, $ZnSnP_2$ is a promising material for low-cost and high

efficiency solar cells.

The preparation of $ZnSnP_2$ thin films was reported by several methods such as co-evaporation [5], chemical vapor deposition (CVD) [6], molecular beam epitaxy (MBE) [7] and liquid phase epitaxy (LPE) [8]. The co-evaporation method has difficulties in controlling the composition at the stoichiometric ratio of $ZnSnP_2$. The CVD and MBE methods use $PH_3$ gas, which is toxic to humans. The LPE method requires a high temperature to grow $ZnSnP_2$, which is not suitable for fabricating thin films on a glass substrate. We therefore adopted a phosphidation method for fabricating $ZnSnP_2$ thin films from an analogy of selenization, in which Cu-In-Ga films react with selenium gas or selenium hydride gas to form $CuIn_{1-x}Ga_xSe_2$. [9] Zn-Sn precursor thin films prepared on a substrate react with phosphorus gas in the phosphidation method, which is suitable for an industrialized process. However, there are no reports of fabricating $ZnSnP_2$ thin films by this method.

In this study, we thus tried to establish phosphidation conditions to obtain thin films with a single $ZnSnP_2$ phase. In particular, the influence of phosphidation temperature on the product phases and the morphology of films was investigated and their changes during phosphidation were discussed from thermodynamics based on the chemical

potential diagram of the Zn-Sn-P system.

## 2. Experimental procedure

### 2.1. Preparation of Zn-Sn thin films

Zn-Sn precursor thin films were prepared on Mo-coated soda lime glass by co-sputtering Zn and Sn using a magnetron sputtering system. The thicknesses of Mo and Zn-Sn thin films were 0.3 and 0.5 μm, respectively. The deposition was carried out at room temperature with a 12 rpm rotation rate of the sputtering stage. In the phosphidation experiments, Zn-Sn thin films are heated to react with phosphorus gas. In the thin films, the composition ratio of Zn/Sn was controlled at about 1.2, because of the higher vapor pressure of Zn compared to Sn. The thickness and composition were measured by inductively coupled plasma atomic emission spectroscopy (ICP-AES), (SII Nano Technology SPS3520UV). Morphology of the films was observed by field emission scanning microscopy (FE-SEM), (HITACHI High Technologies SU6600) and elemental mapping was carried out by energy dispersive X-ray

spectroscopy (EDX), (Oxford Instruments X-MAX20)

### .2.2. Phosphidation of Zn-Sn thin films

For processing thin films by phosphidation, we chose a phosphorus source with two phases, Sn and $Sn_4P_3$, because of the difficulties in controlling phosphorus vapor pressure from red phosphorus.[10] The phosphorus vapor pressure was controlled by heating the phosphorus source.[11] The equilibrium is as shown in equation (1).

$$4\ Sn\ (l) + 3/4\ P_4\ (g) = Sn_4P_3\ (s). \quad (1)$$

The phosphidation apparatus is shown in Fig. 1. Two electric furnaces were used, for the Zn-Sn thin films and the phosphorus source ($Sn/Sn_4P_3$ mixture), respectively, in order to control the temperatures individually. Before phosphidation, the Zn-Sn thin film and the phosphorus source were located at the outer edges of the furnaces in the quartz tube. Initially, the quartz tube was evacuated to $10^{-1}$ Pa and purged with Ar. The two furnaces were then heated to predetermined temperatures under Ar gas flow of 20 sccm, and the phosphorus source was moved into the furnace. In this study, the vapor pressure of phosphorus gas was held at $10^{-2}$ atm, which was determined by the 500 °C temperature of the source furnace. After 15 min to achieve stability, the Zn-Sn thin film was inserted into the furnace and reacted with phosphorus gas. The Zn-Sn

thin film after phosphidation was either cooled down in the furnace, or quenched outside the furnace but in the quartz tube. In the phosphidation experiments, Ar gas was deoxidized by passing through a furnace at 900 °C containing Ti sponge, as shown in Fig. 1. Morphologies and compositions of the thin films before and after phosphidation were analyzed by scanning electron microscopy (SEM), (KEYENCE VE-7800), FE-SEM and EDX (EDAX VE-9800 and Oxford Instruments X-MAX20). The product phases were identified by X-ray diffraction (XRD), (PANalytical X'Pert-ProMPD).

## 3. Results

### 3.1. Zn-Sn precursor thin films fabricated by co-sputtering

Figures 2 shows a surficial SEM image of the Zn-Sn precursor thin film and the corresponding EDX elemental mappings of Zn and Sn. It is observed that Zn and Sn particles were spatially separated from each other and the Sn particles were larger than the Zn. We attribute the morphology of thin film with Zn and Sn separated to the fact that the Zn-Sn system is described by a eutectic phase diagram.

### 3.2. Influence of phosphidation temperature

In order to determine the fabrication conditions for $ZnSnP_2$ thin films with a single phase, the phosphidation experiments were carried out at various temperatures. In the experiments, the phosphidation time was fixed at 30 min. Each sample was cooled in the furnace after phosphidation. Figure 3 shows XRD profiles of the thin films before and after phosphidation. In the samples prepared at lower phosphidation temperatures, e.g., 350 and 400 °C, both $Zn_3P_2$ and $Sn_4P_3$ were identified as secondary phases in addition to $ZnSnP_2$. The thin film after phosphidation at 450 °C contains only $Zn_3P_2$ besides $ZnSnP_2$. In contrast, a single $ZnSnP_2$ phase was successfully obtained in the sample prepared at 500 °C.

From the SEM image of each sample shown in Fig. 4, particles were observed on the surface of thin films prepared at lower temperatures. In contrast, protrusions formed at higher temperatures. The compositions of samples after phosphidation were analyzed using EDX. The average and standard deviation of their compositions are summarized in Table 1. In the sample prepared at 500 °C, the compositions of the protrusions and the surface are close to the stoichiometric ratio of $ZnSnP_2$. This is consistent with the results of XRD shown in Fig. 3. The reason for excessive

phosphorus might be adherence of phosphorus to thin films during cooling in the furnace. The composition of the protrusions observed in the sample prepared at 450 °C is similar to those at 500 °C. In addition, the composition of the surface, in the sample prepared at 450 °C, is Zn-rich compared to the stoichiometric ratio of $ZnSnP_2$. This is attributed to the presence of $Zn_3P_2$ as a secondary phase. On the other hand, the composition of particles observed in samples prepared at 350 and 400 °C is Zn-deficient. Considering the results of XRD, it is indicated that particles are mainly composed of $Sn_4P_3$. Assuming the existence of $ZnSnP_2$, $Zn_3P_2$, and $Sn_4P_3$ in the surface region of thin films prepared at the lower temperatures, their molar fractions were calculated from the EDX analysis to be about 0.70, 0.15, and 0.15, respectively. Therefore, it is concluded that the surface is mainly composed of $ZnSnP_2$, with $Zn_3P_2$ and $Sn_4P_3$ as secondary phases.

### 3.3. Time dependence of phosphidation

Protrusions and particles on the surface of thin films are obstacles to fabricating photovoltaic devices using $ZnSnP_2$. Hence, their growth mechanism should be understood in order to improve the thin films' surface morphology. Here, we carried out phosphidation of the Zn-Sn thin film for only 5 min at 450 °C to investigate the

change of product phases and morphology. This sample was quenched by moving it outside the furnace in the quartz tube. After the 5 min phosphidation, $ZnSnP_2$, $Zn_3P_2$ and Sn were identified from the XRD profile in Fig. 5; however, Zn was not observed. Finally, after 30 min phosphidation, almost single phase of $ZnSnP_2$ were observed. The change of phases between the 5 and 30 min samples can be understood from the reaction between $Zn_3P_2$(s), Sn (l) and $P_4$ (g) to produce $ZnSnP_2$, which is expressed by equation (2).

$$1/3\ Zn3P2\ (s) + Sn\ (l) + 1/3\ P4\ (g) = ZnSnP2\ (s). \quad (2)$$

In the initial stage, it is expected that Zn (l) has reacted with $P_4$ (g) to produce $Zn_3P_2$ (s) according to equation (3),

$$3\ Zn\ (l) + 1/2\ P4\ (g) = Zn3P2\ (s). \quad (3)$$

and subsequently, $Zn_3P_2$ or Zn reacts with Sn and $P_4$ to form $ZnSnP_2$ during the 5 min phosphidation experiment. Thermodynamic considerations in the phosphidation reaction route will be discussed later.

Figure 6 and Table 2 show the SEM images and the EDX analysis of the samples for 5 and 30 min phosphidation, respectively. Some particles were observed on the surface of the thin film prepared for 5 min. From the EDX analysis, the composition

of the particles is Sn-rich. The morphology of this sample is similar to the thin film prepared at lower phosphidation temperatures, such as 350 and 400 °C, shown in Fig. 4. In comparison, protrusions of $ZnSnP_2$ were observed in the sample prepared for 30 min. From these changes, it is expected that the particles with a high concentration of Sn changed to $ZnSnP_2$ protrusions during phosphidation.

## 4. Discussion

### 4.1. Thermodynamic consideration of the phosphidation reaction using chemical potential diagrams

Here, we consider the reaction route where $ZnSnP_2$ thin films with a single phase were obtained to investigate whether there are conditions for fabricating thin films without protrusions. The experimental results are discussed from the viewpoint of thermodynamics using the chemical potential diagram. The review on a chemical potential diagram is summarized by Yokokawa.[12] A chemical potential diagram represents a stable potential region of various substances using chemical potentials of constituent elements as axes. In this work, the chemical potential diagram of the Zn-Sn-P system was created using the software Chesta 2 [13] using the thermodynamic database of Barin [14] and data reported by Arita and Kamo [11]. And we calculated

the standard Gibbs energy of formation of $ZnSnP_2$ using the enthalpy and entropy reported by our group.[15] In this study, the Zn-Sn alloy was not considered for simplification.

Figure 7 shows the chemical potential diagrams at various temperatures. The axes are the logarithms of the partial pressures of Zn (g), Sn (g), and $P_4$ (g), which represent their chemical potentials. The dotted line shows the partial pressure of $P_4$ (g) in the experiments of this study. We here consider the phosphidation behavior at a single temperature for simplicity, although the Zn-Sn thin films were inserted into a furnace that was already heated and the temperature at the thin films was increasing for a time during the actual experiments.

We will discuss the phosphidation of Zn-Sn thin films at 450 °C as an example. Before phosphidation, the thermodynamic coordinates of the Zn-Sn thin film specify the point A in Fig. 7 (c). The chemical potential of phosphorus increases as phosphidation proceed and Zn (l) reacts with $P_4$ (g) to produce $Zn_3P_2$ at the point B, following equation (3). At this point, Zn (l), Sn (l) and $Zn_3P_2$ (s) thermodynamically coexist. The chemical potential of phosphorus then increases along the line between Sn (l) and $Zn_3P_2$ (s), and $ZnSnP_2$ (s) forms at point C, following equation (2). At this

point in the diagram, $ZnSnP_2$ (s) is in equilibrium with $Zn_3P_2$ (s) and Sn (l), which we experimentally observed (see Fig. 5) in the 5 min phosphidation sample. As phosphidation proceeds from point C, there are two possible routes: $ZnSnP_2$ (s) is in equilibrium with $Zn_3P_2$ (s), when Sn (l) is consumed by the $ZnSnP_2$ formation reaction, given by equation (2). Alternatively, excessive Sn (l) leads to the coexistence of $ZnSnP_2$ (s) and Sn (l). Finally, the chemical potential of $P_4$ (g) reaches $10^{-2}$ atm, shown in point D, maintaining the equilibria of $ZnSnP_2$ (s) and $Zn_3P_2$ (s) in the former route. In contrast, $ZnSnP_2$ (s) is in equilibrium with $Sn_4P_3$ (s), shown in point E, where $Sn_4P_3$ is more stable than Sn (l) at the phosphorus potential of $10^{-2}$ atm in the latter case. In this study, the composition of Zn-Sn thin films was Zn-rich, which corresponds to the former case. As shown in the XRD data of Fig. 5, the experimental results of phosphidation at 450 °C are consistent with the above thermodynamic considerations from the chemical potential diagram. However, a single-phase $ZnSnP_2$ thin film was obtained in phosphidation at 500 °C, in spite of the Zn-rich composition in the precursor thin films. In this case, it is expected that evaporation of Zn occurred due to the high phosphidation temperature, and residual $Zn_3P_2$ was not identified, although the same reaction route is considered possible at 450°C from the chemical potential

diagram. On the other hand, $Zn_3P_2$ and $Sn_4P_3$ were experimentally observed as secondary phases in the lower temperature phosphidation samples, but $ZnSnP_2$ (s), $Zn_3P_2$ (s) and $Sn_4P_3$ (s) are not in equilibrium on the chemical potential diagram. This inconsistency results from the driving force for $Sn_4P_3$ formation, which is represented by the difference between the equilibrium potential of $Sn/Sn_4P_3$ and the phosphorus potential of $10^{-2}$ atm, being higher at lower phosphidation temperatures. Therefore, it is concluded that Sn (l) reacted with $P_4$ (g) to produce $Sn_4P_3$ (s) prior to formation of $ZnSnP_2$ (s), while the reaction between $Sn_4P_3$ (s), $Zn_3P_2$ (s) and $P_4$ (g) is assumed to be kinetically difficult because it involves two solid state phases.

**4.2. Growth mechanism of protrusions and particles**

To improve the morphology of thin films after phosphidation, the detailed mechanism of protrusion formation must be understood. We thus propose a growth mechanism shown in Fig. 8, based on the experimental results and the reaction route considered using the chemical potential diagram.

As previously mentioned, Zn and Sn particles are spatially separated in as-sputtered Zn-Sn thin films, and the Sn particles are larger than those of Zn, as illustrated in Fig. 8 (a). In the initial stage of phosphidation, Zn preferentially reacts with $P_4$ to produce

$Zn_3P_2$, and some Sn reacts with $Zn_3P_2$ (or Zn) and $P_4$ to form $ZnSnP_2$. From the densities of $Zn_3P_2$ (4.56 g/cm$^3$),[16] and $ZnSnP_2$ (4.53 g/cm$^3$),[3] the ratio of volume expansion caused by the formation of phosphides is expected to be about twofold. Consequently, compressive stress on unreacted Sn results, as illustrated in Fig. 8 (b). In the intermediate stage (Fig. 8 (c)), it is extruded to the thin film surface, relieving the compressive stress. This behavior is similar to the formation of Sn whiskers observed in Sn thin films electroplated on Cu.[17] In this case, compressive stress caused by formation of intermetallic compounds is the driving force for whisker formation. It is also noted that, in our case, Sn is liquid at these temperatures. Finally, Sn particles on the surface react with Zn, which might be in the gas stage generated from $Zn_3P_2$(s) and $P_4$ (g), to produce $ZnSnP_2$ in the form of protrusions similar to the VLS (Vapor-Liquid-Solid) growth method, [18] as shown in Fig. 8 (d). In the cases of lower temperature, although it is possible that Sn particles are phosphided to form $Sn_4P_3$ due to the large driving force at lower temperatures (such as 350 and 400 °C), they are kinetically unreactive with $Zn_3P_2$ as previously discussed. Therefore, protrusions were not observed. Consequently, it is concluded that formation of $ZnSnP_2$ protrusions is attributed to Sn particles formed on the surface of thin films. Based on

the proposed mechanism, Zn-Sn thin films with good spatial-homogeneity should be prepared to suppress the coarsening of Sn grain and obtain a smooth $ZnSnP_2$ surface.

## 5. Conclusions

In this study, thin films with a single phase of $ZnSnP_2$ were successfully fabricated by phosphidation of co-sputtered Zn-Sn thin films at 500 °C under a phosphorus vapor pressure of $10^{-2}$ atm. On the other hand, $Zn_3P_2$ and $Sn_4P_3$ were formed as secondary phases during phosphidation at lower temperatures, and thin films prepared at 450 °C contained $Zn_3P_2$ in addition to $ZnSnP_2$. These experimental results was understood from the viewpoint of thermodynamics based on the chemical potential diagrams of the Zn-Sn-P system. In addition, the reaction route to obtain $ZnSnP_2$ was investigated. It was clarified that Zn preferentially reacts with phosphorus gas to produce $Zn_3P_2$ in the initial stage of phosphidation. Then, Sn reacts with Zn and $P_4$ to form $ZnSnP_2$ in the case of the higher phosphidation temperatures. In contrast, the formation of $Sn_4P_3$ before $ZnSnP_2$ is considered at lower phosphidation temperatures due to its lager driving force. The reaction between $Zn_3P_2$ and $Sn_4P_3$ might be kinetically difficult, and these two phases were thus observed in the case of lower temperatures.

Some protrusions were observed on the surface of the thin films with a single phase of $ZnSnP_2$ after phosphidation, which was unfavorable for solar cell device. The reason for protrusions formation is that particles with high concentration of Sn were produced on the surface of thin films due to the release of the compressive stress created by phosphides at the initial stage of phosphidation. Then, the particles reacted with $Zn_3P_2$ and phosphorus gas to form $ZnSnP_2$ protrusions, which is a similar mechanism to the VLS growth mode. The SEM images revealed that the formation of the particles was attributed to the morphology of the sputtered Zn-Sn thin film, where Zn and Sn particles were spatially separated and Sn grains are larger than those of Zn. Therefore, Zn-Sn thin films with a spatially homogeneous composition are needed to improve the surface morphology of thin films after phosphidation.

**Acknowlegement**

This work was financially supported by the JST PRESTO program and the Elements Science and Technology Project from MEXT. The authors thank to Kyoto University Nano Technology Hub in Nanotechnology Platform Project sponsored by MEXT for FE-SEM analysis.

## References


[1] M. A. Green, K. Emery, Y. Hishikawa, W. Warta, E. D. Dunlop, Solar cell efficiency table (version 43), Prog. Photovolt: Res. Appl. 22 (2014) 1-9.

[2] W. Wang, M. T. Winkler, O. Gunawan, T. Gokmen, T. K. Todorov, Y. Zhu, D. B. Mitzi, Device Characteristics of CZTSSe Thin-Film Solar Cells with 12.6 % Efficiency, Adv. Energy Mater. (2013), doi: 10.1002/aenm.201301465.

[3] J. L. Shay, J. H. Wernick, Ternary Chalcopyrite Semiconductors: Growth, Electronic Properties, and Applications, Pergamon, Oxford, 1975.

[4] W. Shockley, H. J. Queisser, Detailed Balance Limit of Efficiency of pn Junction Solar Cells, J. Appl. Phys. 32 (1961) 510-519.

[5] H. Y. Shin, P. K. Ajmera, Characterization of Vacuum Grown Thin Films of $ZnSnP_2$, Mater. Lett. 5 (1987) 211-214.

[6] J. Sansregret, The Growth of Thin Films of Zinc Tin Phosphide, Mater. Res. Bull. 16 (1981) 607-611.

[7] G. A. Seryogin, S. A. Nikishin, H. Temkin, A. M. Mintairov, J. L. Merz, M. Holtz, Order-disorder transition in epitaxial $ZnSnP_2$, Appl. Phys. Lett. 74 (1999) 2128-2130.

[8] G. A. Davis, C. M. Wolfe, Liquid Phase Epitaxial Growth of $ZnSnP_2$ on GaAs, J. Electrochem. Soc. 130 (1983) 1408-1412.

[9] S. Niki, M. Contreas, I. Repins, M. Powalla, K. Kushiya, S. Ishizuka, K. Matsubara, CIGS absorbers and processes, Prog. Photovolt: Res. Appl.18 (2010) 453-466.

[10] K. J. Bachmann, E. Buehler, Phase Equilibria and Vapor Pressures of Pure Phosphorus and of the Indium/Phosphorous System and Their Implications Regarding Crystal Growth of InP, J. Electrochem. Soc. 121 (1974) 835-846.

[11] M. Arita, K. Kamo, Measurement of Vapor Pressure of Phosphorous over Sn-P Alloys by Dew Point Method, Trans. JIM. 26 (1985) 242-250.

[12] H. Yokokawa, Generalized Chemical Potential Diagram and Its Applications to Chemical Reactions at Interfaces between Dissimilar Materials, J. Phase Equillib. 20 (1999) 258-287.

[13] N. Hatada, Chesta: Software for Creating Chemical Potential Diagrams http://www.aqua.mtl.kyoto-u.ac.jp/chesta.html Accessed 11 September, 2014.

[14] I. Barin, Thermochemical Data of Pure Substances, third ed., VCH Verlagsgesellschaft mbH, Weinheim, 1995.

[15] Y. Nose, N. Tanaka, T. Uda, in preparation.

[16] I. E. Zanin, K. B. Aleinikova, M. M. Afanasiev, M. Yu. Antipin, Structure of $Zn_3P_2$, J. Struct. Chem. 45 (2004) 844-848.

[17] K. N. Tu, J. C. M. Li, Spontaneous whisker growth on lead-free solder finishes, Mater. Sci. Eng.409, (2005) 131-139.

[18] R. S. Wagner, W. C. Ellis, Vapor-Liquid-Solid Mechanism of Single Crystal Growth, Appl. Phys. Lett. 4 (1964) 89-90.

**Table Captions**

Table 1. EDX composition of thin films after phosphidation at various temperatures.

Table 2. EDX composition of thin films after phosphidation for specified times.

**Figure Captions**

Figure 1. Schematic illustration of phosphidation apparatus.

Figure 2. (a) SEM image of surficial Zn-Sn thin film, and elemental mappings of (b) Zn and (c) Sn.

Figure 3. XRD profiles of Zn-Sn thin films before and after phosphidation for 30 min at various temperatures.

Figure 4. SEM images of thin films (a) before and after phosphidation at (b) 350, (c) 400, (d) 450, and (e) 500 °C

Figure 5. XRD profiles of Zn-Sn thin films before and after phosphidation at 450 °C for 5 and 30 min

Figure 6. SEM images of thin films (a) before and after phosphidation at 450 °C for (b) 5 min and (c) 30 min.

Figure 7. Chemical potential diagrams of Zn-Sn-P system at (a) 350, (b) 400, (c) 450, and (d) 500 °C.

Figure 8. Growth mechanism of $ZnSnP_2$ protrusions: (a) Before phosphidation, (b) initial and (c) intermediate stage of phosphidation, and (d) after phosphidation.

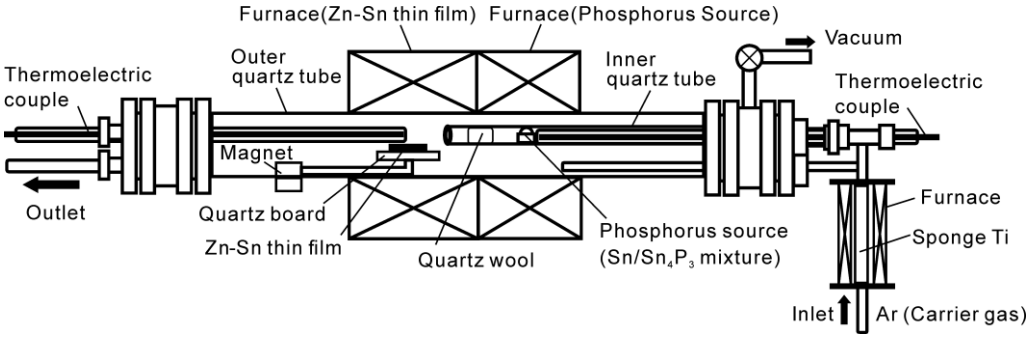


Fig.1

Nakatsuka et al.

(a)

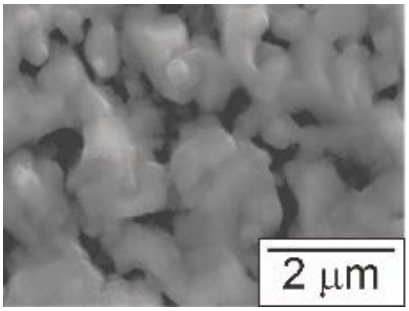


(b)

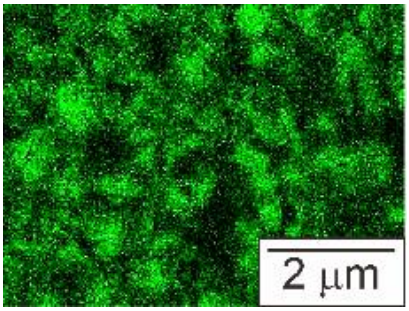


(c)

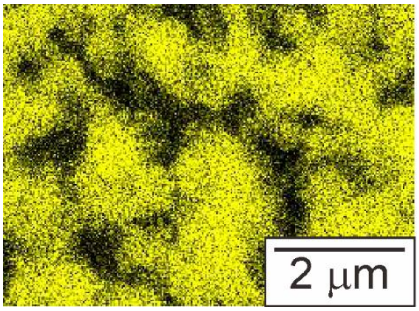


Fig.2

Nakatsuka et al.

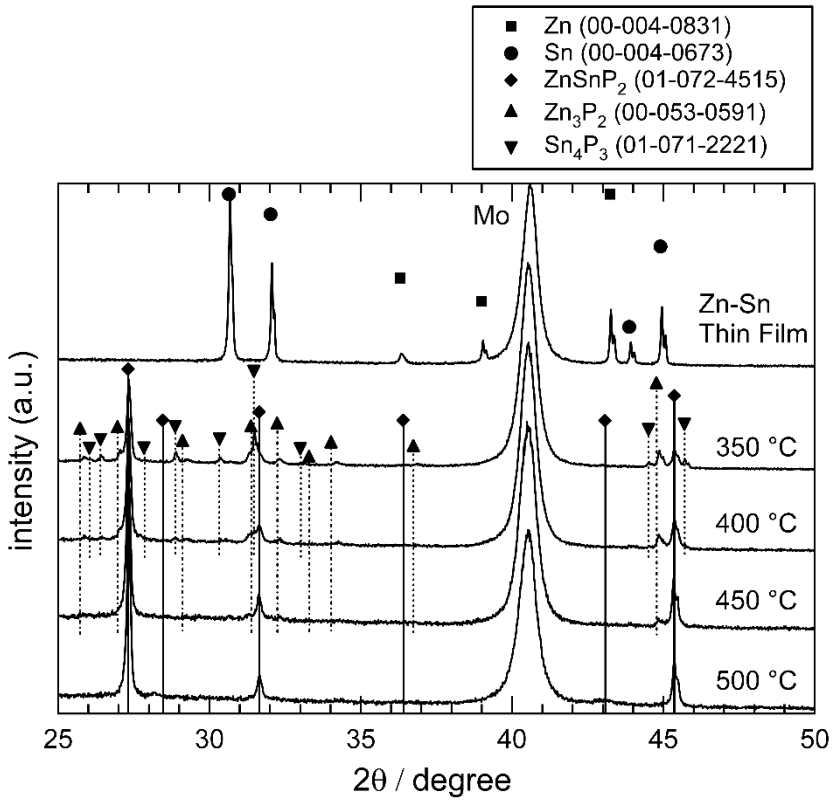


Fig.3

Nakatsuka et al.

(a)

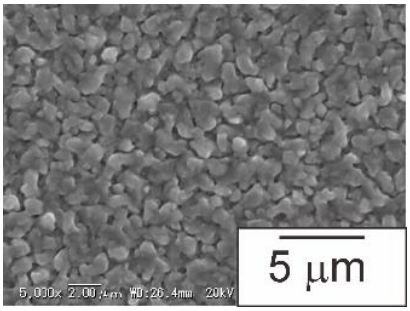


(b)

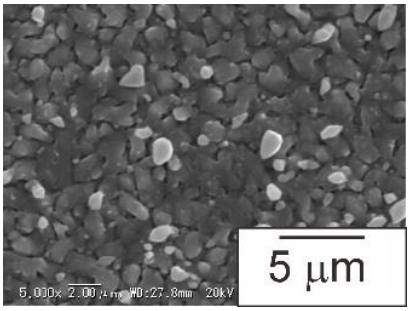


(c)

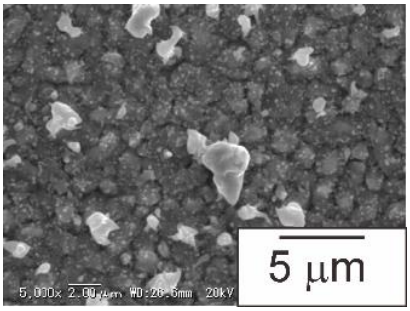


(d)

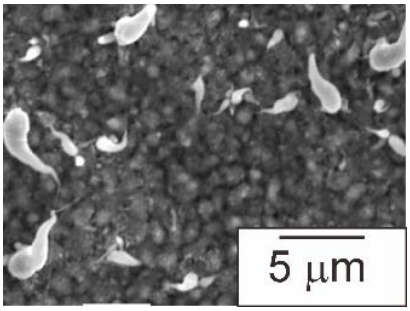


(e)

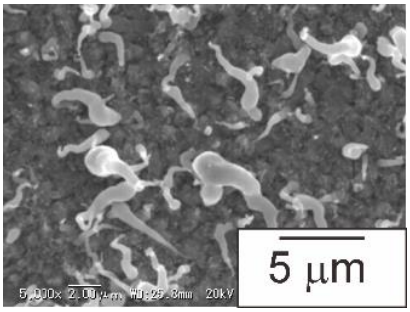


Fig.4

Nakatsuka et al.

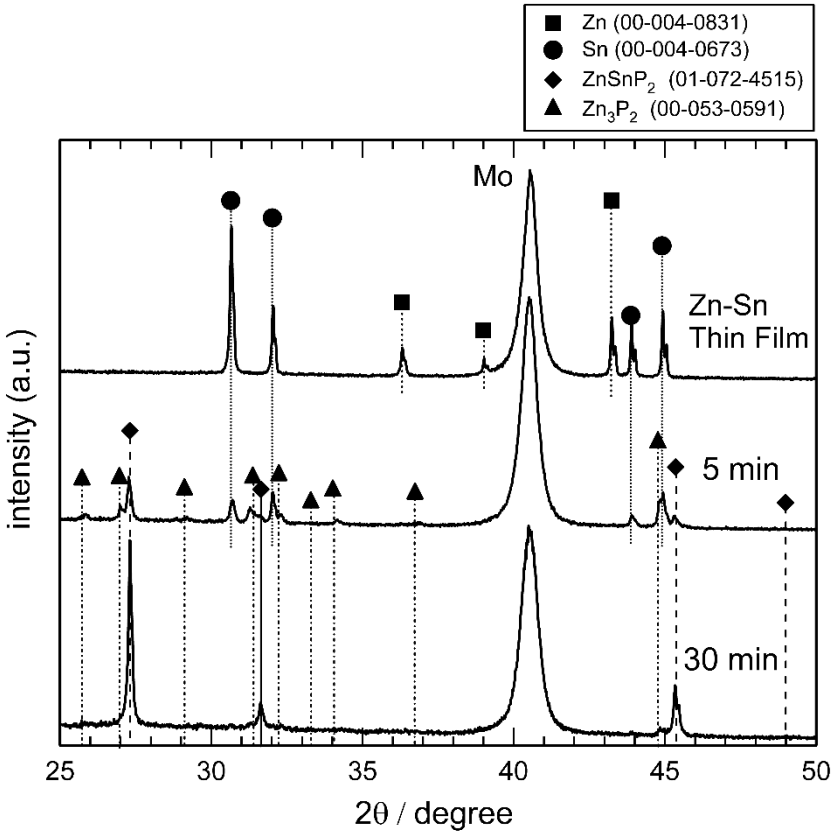


Fig.5

Nakatsuka et al.

(a)

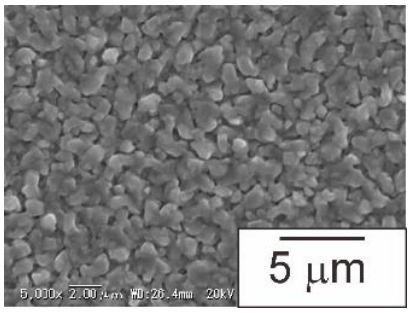


(b)

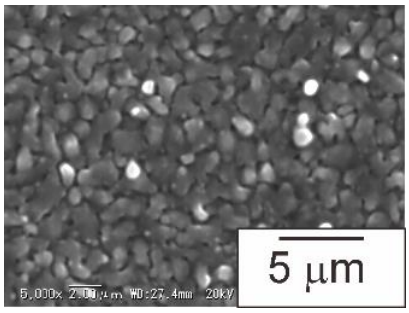


(c)

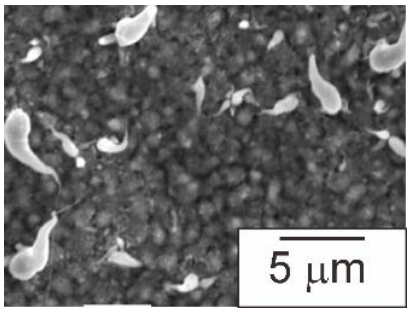


Fig.6

Nakatsuka et al.

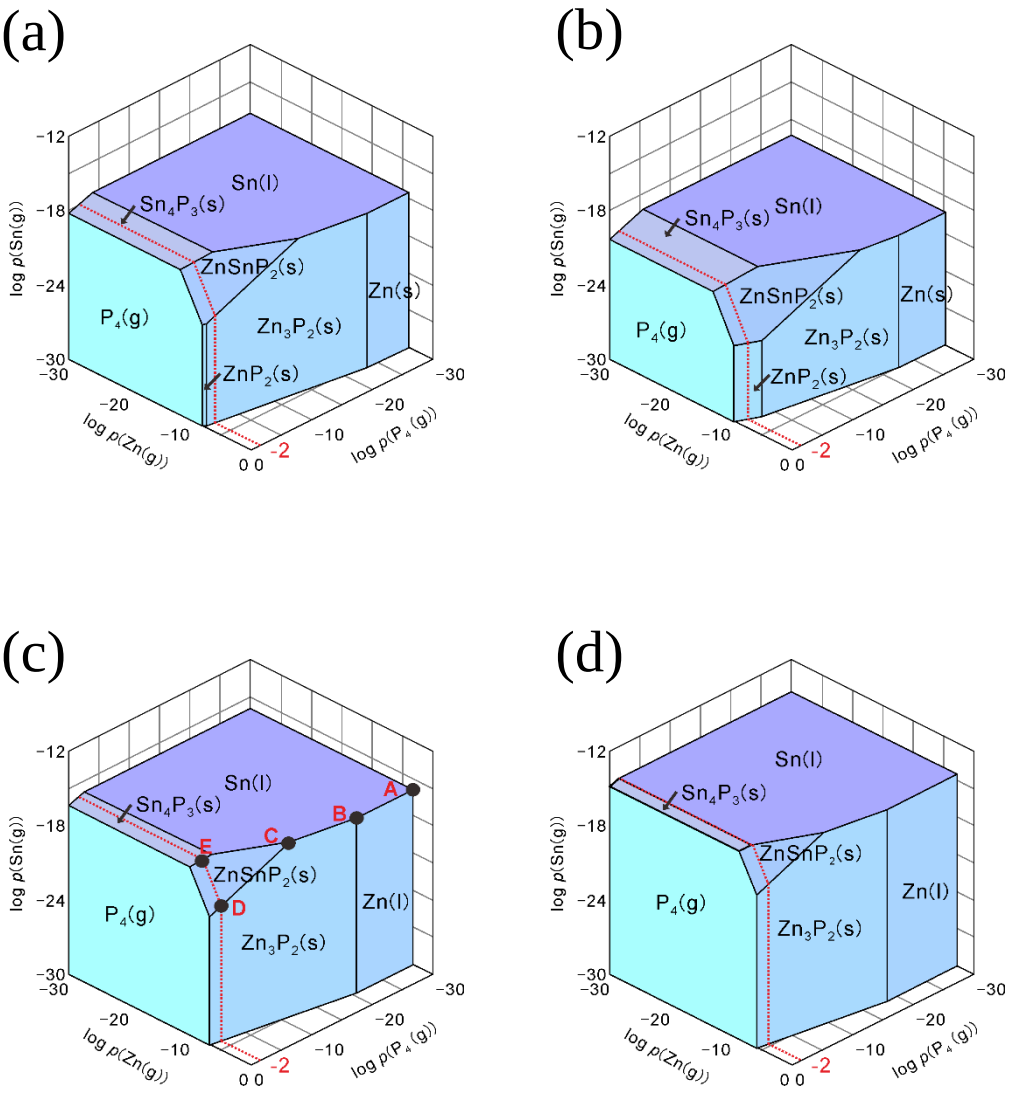


Fig.7

Nakatsuka et al.

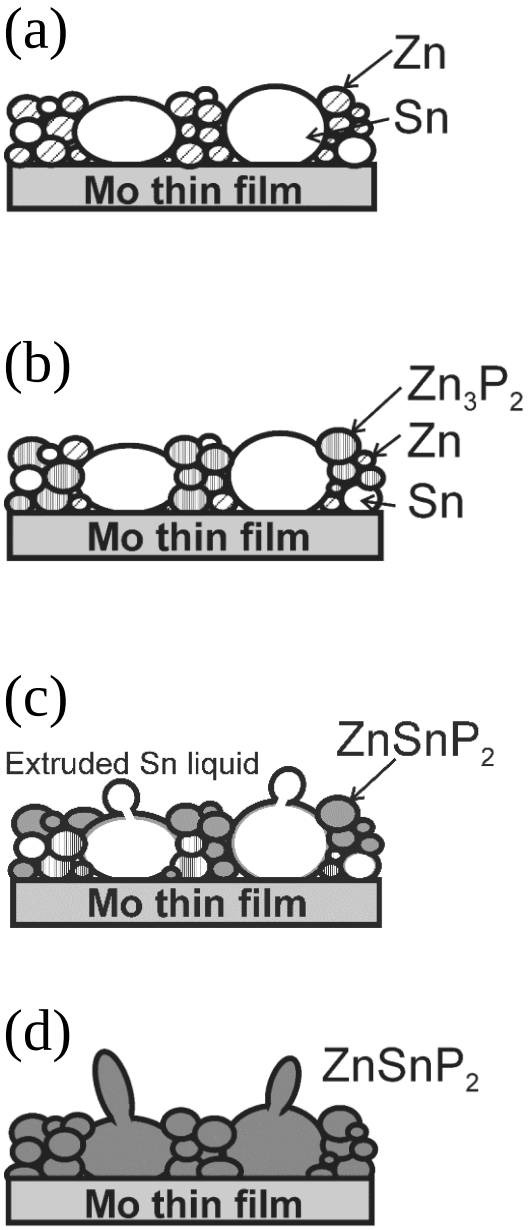


Fig.8

Nakatsuka et al.